XLIII CILAMCE
21–25, November, 2022
FOZ DO IGUAÇU – PR – BRAZIL

# A Modified Drucker-Prager Cap Plasticity Model for Triaxial Simulation of Residual Soils

Fernando Fante[1], Maria Mariana de S. Rocha[1], Gracieli Dienstmann[2], Cesar A. Ruver[1], Nilo C. Consoli[1]

[1] *Department of Civil Engineering, Federal University of Rio Grande do Sul*
*Avenida Osvaldo Aranha, 99 - Centro Histórico, 90035-190, Porto Alegre, Brasil*
*nandofante@gmail.com, mariamarianasousa1@gmail.com, cesar@ufrgs.br, consoli@ufrgs.br*
[2] *Department of Civil Engineering, Federal University of Santa Catarina*
*Rua João Pio Duarte da Silva, 205 – Córrego Grande, 88037-000, Florianópolis, Brasil*
*g.dienstmann@gmail.com*

**Abstract.** A large area of Brazil, even as the world, is covered by residual soils. These soils arise as the result of the weathering process of the intact rock and are characterized by the permanence of fragmented elements at the site of formation. The accuracy of a numerical simulation depends on the adequacy of the model and its parameters to the soil behavior. In this context, this research aims to numerically evaluate triaxial tests of residual soils to assess the influence of the model parameters on the stress-strain-volumetric response. The analysis was performed using ABAQUS software, in which an elastic-plastic model with Drucker-Prager failure criteria and CAP plasticity was used. The numerical response was compared with a laboratory test in which confining stresses of 20 kPa, 35 kPa, and 50 kPa were employed. A sensitivity analysis of the parameters of the model was performed. The results indicated that the studied model showed a satisfactory prediction of stress-strain-volumetric behavior of the residual soil. In the sensitivity analysis, the cohesion, friction angle, cap eccentricity, and hydrostatic yield stress parameters presented more impact in the numerical response.

**Keywords:** residual soils, numerical simulation, laboratory tests, bonded soils.

## 1 Introduction

Residual soils are formed when the velocity of weathering and decomposition of the rock is greater than the velocity of transport of the degraded particles; thus resulting in the soil remaining where it was generated (HUAT [1]; BLIGHT [2]). These soils cover extensive areas located in tropical and subtropical regions – mainly under hot and humid conditions – where the conditions favor the intense hydrolysis processes that cause the decomposition of minerals at great depths (GIDIGASU [3]; DIAS [4]). Moreover, residual soils are strongly dependent on their formation process and their natural bonded structure, and as a consequence, there is a particular difficulty in reconstituting soil samples in the laboratory (BOGADO [5]). In this context, the numerical analysis may contribute to the understanding of the stress state in the soil mass and of the mechanisms that control its behavior. Furthermore, the use of appropriate parameters has a fundamental importance in achieving a more representative analysis. This work aims to numerically simulate triaxial tests of residual soils to study the influence of the model parameters on the stress-strain-volumetric response of the soil and to establish the best fit set of parameters.

## 2 Constitutive model

The numerical analysis was conducted employing the modified Drucker-Prager cap plasticity model (MDPC). In this aspect, the yield surface used in the MDPC was defined in terms of stress invariants: equivalent pressure stress ($p$), Mises equivalent stress ($q$), and third invariant of deviatoric stress ($r$) (SIMULIA [6]), and presented in eq. (1), (2), and (3), respectively.

$$p = -\frac{1}{3} trace(\boldsymbol{\sigma}). \tag{1}$$

$$q = \sqrt{\frac{3}{2}(\boldsymbol{S}:\boldsymbol{S})}. \tag{2}$$

$$r = \left(\frac{9}{2}\boldsymbol{S}\cdot\boldsymbol{S}:\boldsymbol{S}\right)^{\frac{1}{3}}. \tag{3}$$

The stress deviator (**S**) is presented as:

$$\boldsymbol{S} = \boldsymbol{\sigma} + p\boldsymbol{I}. \tag{4}$$

Where ($\boldsymbol{\sigma}$) is the stress tensor, and **I** is the identity matrix. Moreover, the deviatoric stress measure ($t$) is a function of the second ($q$) and third ($r$) invariants, and with the flow stress ratio ($K$) as given (SIMULIA [6]):

$$t = \frac{q}{2}\cdot\left[1 + \frac{1}{K} - \left(1 - \frac{1}{K}\right)\cdot\left(\frac{r}{q}\right)^3\right]. \tag{5}$$

In this respect, the flow stress ratio ($K$) controls the yield dependence on the third invariant of the deviatoric stress ($r$) and permits different shapes in the deviatoric plane (SIMULIA [6]). The yield surface of the MDPC is formed by three parts: Drucker-Prager shear failure surface ($F_s$), cap yield surface ($F_c$), and transition yield surface ($F_t$), as presented in Fig. 1a.

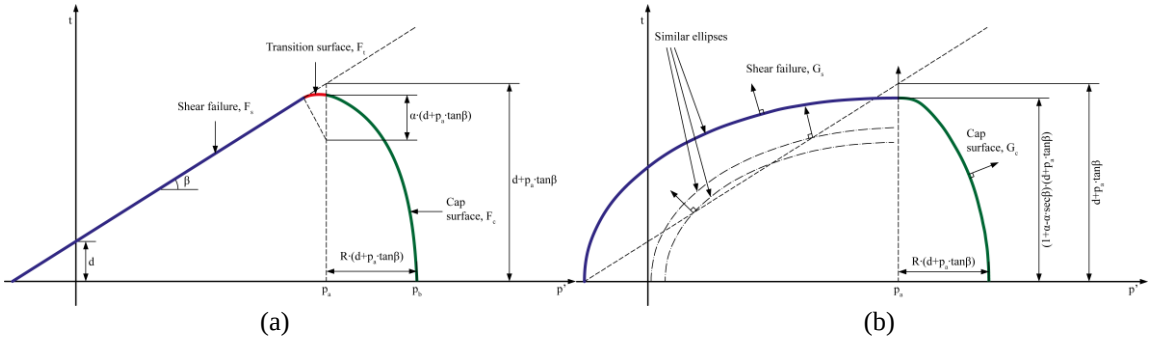


Figure 1. Modified Drucker-Prager Cap Plasticity model: (a) yield surfaces in the meridional plane; (b) flow potential in the meridional plane.

In this regard, the Drucker-Prager shear failure surface ($F_s$) is given by (SIMULIA [6]):

$$F_s = t - p\cdot tan\,\beta - d = 0. \tag{6}$$

Where ($\beta$) is the material friction angle in the $t - p$ plane, and ($d$) is the material cohesion in the $t - p$ plane, as shown in Fig. 1a. The cap yield surface ($F_c$) hardens (expands) or softens (shrinks) as a function of the volumetric plastic strain and is defined by (SIMULIA [6]):

$$F_c = \sqrt{[(p - p_a)]^2 + \left[\frac{R\cdot t}{1+\alpha-\frac{\alpha}{cos\,\beta}}\right]^2} - R\cdot(d + p_a\cdot tan\,\beta) = 0. \tag{7}$$

Where: ($p_a$) is a pressure evolution parameter, ($R$) is the cap eccentricity parameter that controls the shape of the cap, and ($\alpha$) is the transition yield surface radius that defines a smooth changeover between the cap ($F_c$) and shear ($F_s$) surfaces. In addition, the pressure evolution parameter ($p_a$) is defined as (SIMULIA [6]):

$$P_a = \frac{p_b - R\cdot d}{(1+R\cdot tan\,\beta)}. \tag{8}$$

Where: ($p_b$) is the hydrostatic yield stress and is directly related to the hardening law. In this regard, the hardening law can be constructed by the relation between the hydrostatic yield stress ($p_b$) and plastic volumetric strain ($\varepsilon_v$) according to eq. 9 (HELWANY [7]):

$$\varepsilon_v^p = \frac{C_c - C_s}{2.3 \cdot (1+e_0)} \cdot ln \frac{p}{p_b}. \tag{9}$$

Where: ($p$) is the mean stress, ($e_0$) is the initial void ratio, ($C_c$) is the coefficient of compression, and ($C_s$) is the coefficient of recompression.

The initial position of the cap yield surface is defined by the initial inelastic volumetric strain on the hydrostatic axis (SIMULIA [6]). Naturally, as the cap increases its size, more pressure is necessary to cause a plastic strain, and it is controlled by the hardening law (SHIN [8]). Thus, the initial inelastic volumetric strain was adopted to $\varepsilon_v^{in} = 0$, which means that the plastic deformation starts with the hydrostatic yield stress ($p_b$).

Finally, the transition yield surface ($F_t$) is given by (SIMULIA [6]):

$$F_t = \sqrt{[(p - p_a)]^2 + \left[t - \left(1 - \frac{\alpha}{cos\,\beta}\right) \cdot (d + p_a \cdot tan\,\beta)\right]^2} - \alpha \cdot (d + p_a \cdot tan\,\beta) = 0. \tag{10}$$

On the other hand, the flow potential assumes an associated flow rule in the cap yield surface and a nonassociated flow rule in the failure and transition surfaces (SIMULIA [6]). The flow potential ($G_c$) in the cap region and the flow component ($G_s$) in the failure and transition regions are given by eq. (11) and (12), respectively:

$$G_c = \sqrt{[(p - p_a)]^2 + \left[\frac{R \cdot t}{1 + \alpha - \frac{\alpha}{cos\,\beta}}\right]^2}. \tag{11}$$

$$G_s = \sqrt{[(p_a - p) \cdot tan\,\beta]^2 + \left[\frac{t}{1 + \alpha - \frac{\alpha}{cos\,\beta}}\right]^2}. \tag{12}$$

The flow functions ($G_c$ and $G_s$), form a continuous and smooth potential surface, as illustrated in Fig. 1b.

## 3 Finite element model

To evaluate the soil behavior (*i.e.*, axial strain *versus* deviatoric stress; axial strain *versus* volumetric strain) an axisymmetric finite element analysis was performed using the commercial software package ABAQUS v.6.14. To perform the investigation, an elastic-plastic constitutive model with a Modified Drucker-Prager Cap Plasticity (MDPC) yield criteria was used. The model was formed by a two-dimensional axisymmetric mesh with one element. A pore fluid/stress 8-node axisymmetric quadrilateral, with biquadratic displacement, bilinear pore pressure, and reduced integration element was adopted. The element had a radius of 0.025 m and a height of 0.05 m – which corresponds to only one-quarter of the triaxial soil sample (Fig. 2).

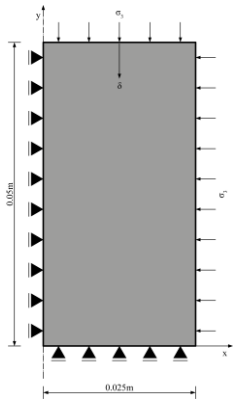


Figure 2. Schematic illustration of the model.

Moreover, a series of boundary conditions were applied in the soil part: (i) the nodes of the bottom mesh were constrained; (ii) a symmetry line was positioned on the left-hand side of the mesh – as illustrated in Fig. 2; (iii) the nodes of the top and the right-hand side were free to displace. The top and bottom of the soil specimen

were pervious, which implies that both may drain during the loading application. A uniform downward displacement of 0.020 m was applied on the top surface of the mesh following a ramp distribution.

The analysis – as was executed in a consolidated drained triaxial test – was divided into two different steps: consolidation and shearing steps. The first step was applied in a single increment where the drainage was open across the top surface. In this step, the confining stresses (20, 35, and 50 kPa) were imposed on the right-hand side and the top of the mesh through a geostatic procedure. This strategy guarantees the equilibrium in the soil specimen and makes sure that the initial stress fails into the initial yield surface (HELWANY [7]). In the second step, a displacement was imposed on the top of the mesh to simulate the movement of the loading plate (see Fig. 2). To ensure that the excess pore pressure within the soil was near zero, a slow rate ($2 \times 10^{-11}$ m/s) was employed. Automatic time stepping with a maximum pore water pressure change of 0.007 kPa was used to certify that the test was fully drained as suggested by Helwany [7].

## 4 Sensitivity analysis

The triaxial soil data employed in this analysis was obtained from Fante *et al.* [9] and was conducted with natural soil samples of residual soil. To conduct the sensitivity analysis, a set of initial parameters which provide the best fit of the soil data was defined. The objective of that procedure was to determine the medium set of parameters, which posteriorly were incremented and decremented at two different levels: high and low, respectively. The levels of the sensitivity analysis for the parameters: material cohesion in the $t - p$ plane ($d$), material friction angle in the $t - p$ plane ($\beta$), hydrostatic compression yield stress ($p_b$), Young's modulus ($E$), and Poisson's ratio ($\upsilon$) were changed in a probable range of occurrence, according to the data available in the literature (e.g., CARRETTA [10]; CARRETTA et al., [11]; DIAS [4]; FANTE [12]; FANTE *et al.* [9]; ROCHA [13]). On the other hand, the parameters: cap eccentricity parameter ($R$); transition yield surface radius ($\alpha$), and flow stress ratio ($K$) were altered in a spectrum that considered previous trials and the possible range of occurrence according to the model (SIMULIA [6]). The parameters used in the hardening law were kept constant due to they are out of the scope of the sensitivity analysis: coefficient of compression $C_c = 0.42$; coefficient of recompression $C_s = 0.025$; initial void index $e_0 = 1.25$; and the mass density $\rho = 1615$ kg/m³. The combinations employed in the sensitivity analysis for all three confinement stresses (20, 35, and 50 kPa) were displayed in Tab. 1. Run 1 represents all the parameters in the intermediate, *i.e.*, medium condition. After that, one factor was changed at a time, for the high and low levels.

Table 1. Combinations of the materials model parameters for the sensitivity analysis.

| Runs | Parameters | | | | | | | |
|---|---|---|---|---|---|---|---|---|
| | $\beta$ (°) | $d$ (kPa) | $E$ (MPa) | $p_b$ (kPa) | $R$ | $\upsilon$ | $K$ | $\alpha$ |
| 1 | 50 | 20 | 40 | 90 | 0.6 | 0.3 | 0.9 | 0.03 |
| 2 | 60 | 20 | 40 | 90 | 0.6 | 0.3 | 0.9 | 0.03 |
| 3 | 40 | 20 | 40 | 90 | 0.6 | 0.3 | 0.9 | 0.03 |
| 4 | 50 | 30 | 40 | 90 | 0.6 | 0.3 | 0.9 | 0.03 |
| 5 | 50 | 10 | 40 | 90 | 0.6 | 0.3 | 0.9 | 0.03 |
| 6 | 50 | 20 | 60 | 90 | 0.6 | 0.3 | 0.9 | 0.03 |
| 7 | 50 | 20 | 20 | 90 | 0.6 | 0.3 | 0.9 | 0.03 |
| 8 | 50 | 20 | 40 | 120 | 0.6 | 0.3 | 0.9 | 0.03 |
| 9 | 50 | 20 | 40 | 60 | 0.6 | 0.3 | 0.9 | 0.03 |
| 10 | 50 | 20 | 40 | 90 | 0.8 | 0.3 | 0.9 | 0.03 |
| 11 | 50 | 20 | 40 | 90 | 0.4 | 0.3 | 0.9 | 0.03 |
| 12 | 50 | 20 | 40 | 90 | 0.6 | 0.4 | 0.9 | 0.03 |
| 13 | 50 | 20 | 40 | 90 | 0.6 | 0.2 | 0.9 | 0.03 |
| 14 | 50 | 20 | 40 | 90 | 0.6 | 0.3 | 1.0 | 0.03 |
| 15 | 50 | 20 | 40 | 90 | 0.6 | 0.3 | 0.8 | 0.03 |
| 16 | 50 | 20 | 40 | 90 | 0.6 | 0.3 | 0.9 | 0.05 |
| 17 | 50 | 20 | 40 | 90 | 0.6 | 0.3 | 0.9 | 0.01 |

To evaluate the influence of the parameter on the predicted response, the sensitivity was approximated using

the relative sensitivity ($S_r$) as given (WHITE [14]):

$$S_r = \left(\frac{x}{y}\right) \cdot \left(\frac{y_2 - y_1}{x_2 - x_1}\right). \tag{13}$$

Where: ($x_2$), ($x$), and ($x_1$), are the parameters at the high, medium, and low levels, and ($y_2$), ($y$), and ($y_1$) are the predicted output at the high, medium, and low levels, respectively. The greater the value of the relative sensitivity, the more sensitive the output variable is to that particular parameter. There are some limitations to the use of ($S_r$) to assess parameters in a model: the assumption of linearity on the parameters' variation, the lack of consideration of the interaction between the parameters, and the lack of examination of the uncertainty associated with each parameter (WHITE [14]). Despite that, the relative sensitivity may provide an idea of which parameters have a greater impact on the calibration of the model. To standardize the analysis, the adopted criterion was that the relative sensitivity was measured at the last point of the numerical analysis, more specifically at $\varepsilon_a$ = 10%. Finally, the numerical data was collected at the mesh element nodes.

## 5 Results and analysis

Figures 3 and 4 present the stress-strain behavior for the numerical analysis of the isotropically consolidated drained triaxial test to the consolidation stress of 35 kPa. It is important to mention that the qualitative behavior of the three stresses (20, 35, and 50 kPa) was the same, for that reason, only the intermediate stress was presented in this discussion. In this aspect, the analysis focus on some key points of the calibration: the initial slope and the final deviatoric stress ($q_{fin}$) on the stress-axial strain behavior and the final volumetric strain ($\varepsilon_{v\ fin}$). The final deviatoric stress and volumetric strain were considered at an axial strain $\varepsilon_a$ = 10%.

The influence of the ($\beta$) parameter (*i.e.*, material friction angle in the $t - p$ plane) on the stress-axial strain and volumetric axial strain is displayed in Fig. 3a and 3e, respectively. It can be seen that an increase in ($\beta$) results in an increase in the final deviatoric stress and the growth of the volumetric strains. When ($\beta$) was decremented – the reverse process occurred – a decrease in the deviatoric stress and the volumetric strains. As expected, the initial slope was not affected by the variation of the ($\beta$) because the parameter does not impact the stiffness. Similar behavior was observed when the influence of the ($d$) parameter (*i.e.*, material cohesion in the $t - p$ plane) on the stress-axial strain (Fig. 3b) and volumetric axial strain (Fig. 3f) was verified.

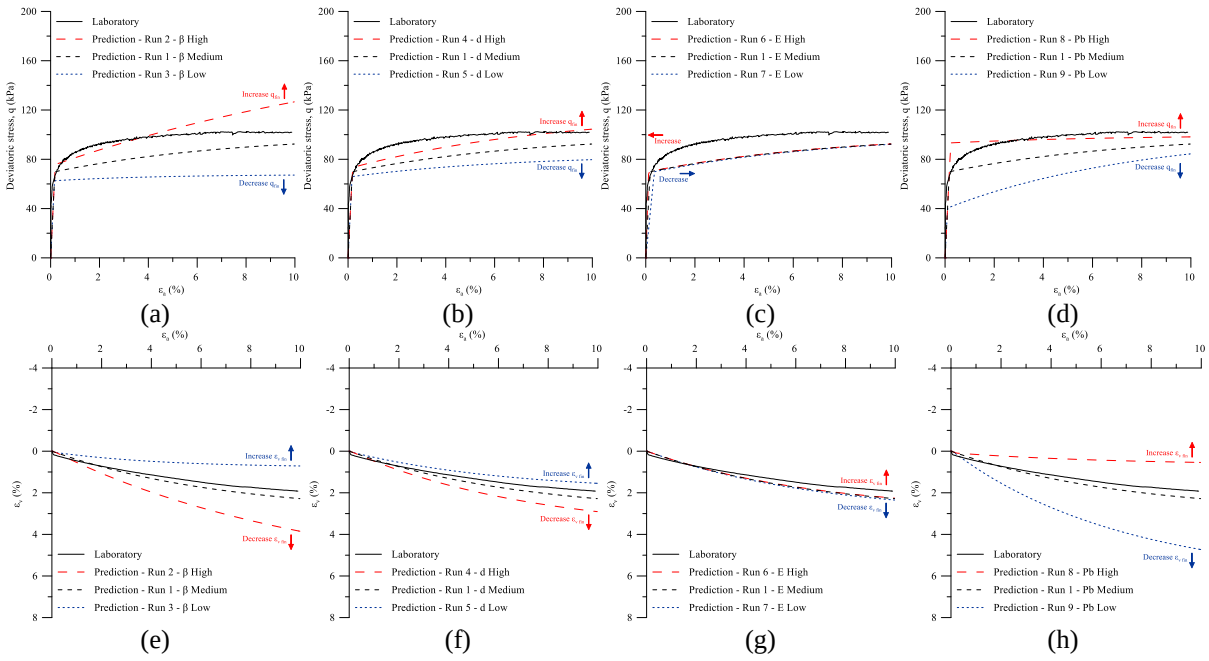


Figure 3. Effect of the parameters $\beta$, $d$, $E$, and $P_b$ in the numerical analysis for the isotropically consolidated drained conventional triaxial tests at confining stress of 35 kPa for bonded residual soil: (a), (b), (c) and (d) deviatoric stress *versus* $\varepsilon_a$; (d), (e), (f) and (g) $\varepsilon_v$ *versus* $\varepsilon_a$.

Otherwise, when the effect of Young's modulus ($E$) was analyzed, an increase at this parameter provides a steeper initial slope on the stress-strain behavior and a decrease leads to a less steep slope (Fig. 3c). The variation on this parameter virtually does not affect the final deviatoric stress. However, a small decrease in the volumetric final strain with the ($E$) parameter at the high level was observed (Fig. 3g). Last, an increase in the level of the ($P_b$) parameter (*i.e.*, hydrostatic compression yield stress) leads to a growth in the final deviatoric stress (Fig. 3d) and a decrease in the volumetric strains (Fig. 3g) due to the increase of the elastic space of the model. When ($P_b$) was reduced, there was a decrease in the final deviatoric stress and a diminution in the initial linear portion of the stress-strain curve – caused by the decrease of the elastic space of the model (see Figure 1a). As the values of ($P_b$) decrease and approach the confinement stress of the test, the linear portion diminishes and presents a behavior similar to normally consolidated soil or loose sand. Additionally, smaller values of ($P_b$) result in greater values of volumetric strains. The changes in the levels of ($P_b$) do not affect the initial slope of the stress-strain curve.

Figures 4a and 4e show the influence of the ($R$) parameter (*i.e.*, cap eccentricity parameter in $t - p$ plane) on the stress-axial strain and volumetric axial strain, respectively. It is interesting to note that an increase in the parameter leads to a decrease in the final deviatoric stress and an increment in the volumetric strains. This occurs due to the reduction in the initial space in the $t - p$ plane (Fig. 1a). The opposite occurs when the parameter is reduced. Moreover, the initial slope was not impacted by the change in the levels of ($R$). Otherwise, when the effect of Poisson's ratio ($v$) was analyzed, an alteration of the levels does not influence the stress-strain response (Fig. 4b). The increase in ($v$) generates only a slight decrease in the volumetric strains (Fig. 4f), and when ($v$) is reduced, the opposite appears. The ($K$) parameter does not provoke any change in the stress-strain-volumetric behavior (see Fig. 4c and 4g). Finally, when the level of the transition yield surface radius ($\alpha$) was changed, there was an increase in the final deviatoric stress (Fig. 4d) and a decrease in the volumetric strains (Fig. 4h) with the increase of the parameter. The initial slope of the stress-strain curve was not affected by the alterations of ($\alpha$).

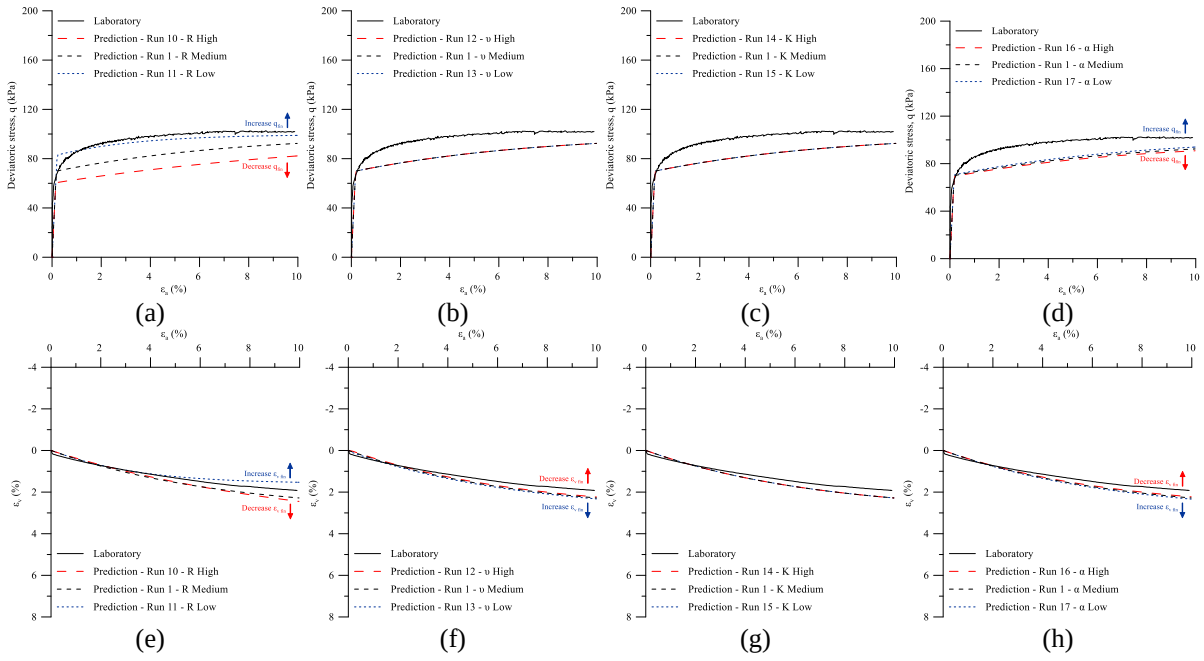


Figure 4. Effect of the parameters, $R$, $v$, $K$, and $\alpha$ in the numerical analysis for the isotropically consolidated drained conventional triaxial tests at confining stress of 35 kPa for bonded residual soil: (a), (b), (c) and (d) deviatoric stress *versus* $\varepsilon_a$; (d), (e), (f) and (g) $\varepsilon_v$ *versus* $\varepsilon_a$.

Table 2. Relative sensitivity of the materials model parameters.

| Variable | Parameters | | | | | | | |
|---|---|---|---|---|---|---|---|---|
| | $\beta$ | $d$ | $E$ | $p_b$ | $R$ | $\upsilon$ | $K$ | $\alpha$ |
| $q_{fin}$ | 1.61 | 0.27 | 0.00 | 0.22 | 0.27 | 0.00 | 0.00 | 0.03 |
| $\varepsilon_{v\,fin}$ | 3.44 | 0.60 | 0.04 | 2.75 | 0.06 | 0.06 | 0.00 | 0.04 |

On the other hand, when the relative sensitivity of the material model parameters was analyzed (Tab. 2), it can be observed that for the final deviatoric stress ($q_{fin}$), the parameters that caused more impact were: material friction angle in the $t - p$ plane ($\beta$) with $S_r = 1.61$, material cohesion in the $t - p$ plane ($d$) with $S_r = 0.27$, cap eccentricity parameter in $t - p$ plane ($R$) with $S_r = 0.27$, and the hydrostatic compression yield stress ($p_b$) with $S_r = 0.22$. For the final volumetric strain ($\varepsilon_{v\,fin}$), the parameters that provoke more impact were: material friction angle in the $t - p$ plane ($\beta$) with $S_r = 3.44$, hydrostatic compression yield stress ($p_b$) with $S_r = 2.75$, material cohesion in the $t - p$ plane ($d$) with $S_r = 0.60$. These findings corroborate what was previously discussed, the effect of each parameter on the stress-axial strain and volumetric-axial strain behavior.

# 6 Conclusions

This study numerically evaluated triaxial tests of residual soils to assess the influence of the model parameters on the stress-strain-volumetric response. In this aspect, the modified Drucker-Prager cap plasticity model provided a reasonable representation of the behavior of the soil. Moreover, the sensitivity analysis showed the parameters of material friction angle, material cohesion, and cap eccentricity parameter in the $t - p$ plane; and the hydrostatic compression yield stress causes the major impact in the stress-strain-volumetric response.

**Acknowledgments.** The authors wish to express their appreciation to FAPERGS/CNPq 12/2014 – PRONEX (Project #16/2551-0000469-2), MCT-CNPq (Editais INCT-REAGEO, Universal & Produtividade em Pesquisa), and MEC-CAPES (PROEX) for the support to the research group.

**Authorship statement.** The authors hereby confirm that they are the sole liable persons responsible for the authorship of this work, and that all material that has been herein included as part of the present paper is either the property (and authorship) of the authors, or has the permission of the owners to be included here.

# References

[1] HUAT, B.B.K; Toll, D.G.; Prasad, A. *Handbook of Tropical Residual Soils Engineering*. London: CCR Press/Balkena, 2013.
[2] BLIGHT, G.E. *Origin, and formation of residual soils*. In: BLIGHT, G.E.; LEONG, E. Mechanics of residual soils. 2. ed: CRC Press, 2012.
[3] GIDIGASU, M. D. *Laterite Soil Engineering: Pedogenesis and Engineering Principles*. Elsevier Scientific Publishing Company, Amsterdam, the Netherlands, 1976.
[4] DIAS, R. D. *Aplicação de Pedologia e Geotecnia no Projeto de Fundações de Linhas de Transmissão*. 1987. Tese (Doutorado) - Instituto Alberto Liz Coimbra de Pós-Graduação e Pesquisa de Engenharia (COPPE), Universidade Federal do Rio de Janeiro, Rio de Janeiro, 1987.
[5] BOGADO, G.O., Reinert H.O., and Francisca F.M. Geotechnical properties of residual soils from the north-east of Argentina. *International Journal of Geotechnical Engineering* 13(2): 112–121, 2019.
[6] SIMULIA. *Abaqus Theory Guide - Version 6.14*. Providence, RI: Dassault Systemes Simulia Corp, 2010.
[7] HELWANY, S. *Applied soil mechanics with ABAQUS applications*. [s.l.]: John Wiley & Sons, Inc., 2007.
[8] SHIN, H. et al. A simulation-based determination of cap parameters of the modified Drucker–Prager cap model by considering specimen barreling during conventional triaxial testing. *Computational Materials Science*, [s. l.], v. 100, p. 31–38, 2015.
[9] FANTE, F. et al. Behaviour of a Weakly Bonded Residual Soil Subjected to Monotonic and Cyclic Loading. *Proceedings of the Institution of Civil Engineers - Geotechnical Engineering*, [s. l.], p. 1–30, 2022.
[10] CARRETTA, M. da S. *Comportamento de um solo residual levemente cimentado: Estimativa de capacidade de carga para estacas submetidas a esforços transversais*. 2018. Dissertação (Mestrado) - Programa de Pós-Graduação em Engenharia Civil, Universidade Federal do Rio Grande do Sul, Porto Alegre, 2018.
[11] CARRETTA, M. da S. et al. Experimental assessment of the small-strain response of residual soil under monotonic and cyclic loading. *Proceedings of the Institution of Civil Engineers - Geotechnical Engineering*, [s. l.], p. 1–14, 2021.
[12] FANTE, F. *Comportamento de Fundações Diretas Submetidas à Carregamento Cíclico em Solo Residual*. 2021. Dissertação (Mestrado) - Programa de Pós-Graduação em Engenharia Civil, Universidade Federal do Rio Grande do Sul, Porto Alegre, 2021.
[13] ROCHA, M. M. de S. *Análise do Comportamento de Fundações Superficiais Submetidas a Carregamentos Excêntricos em um Solo Residual*. 2021. ação em Engenharia Civil, Universidade Federal do Rio Grande do Sul, Porto Alegre, 2021.
[14] WHITE, K. L.; Chaubey, I. Sensitivity analysis, calibration, and validations for a multisite and multivariable SWAT model. *Journal of the American Water Resources Association*, [s. l.], v. 41, n. 5, p. 1077–1089, 2005.